Autumn Rainfall Anomalies and Regional Atmospheric Circulation along Establishment of Weak La Nina after Strong El Nino in Iran

Faranak Bahrami [1], Abbas ranjbar saadatabadi [2*], Amir Hussain Meshkatee [3] and Gholamali Kamali[3]

[1] PhD Student, Department of earth science, Science and Research Branch, Islamic Azad University, Tehran, Iran.
[2] Associate Professor, Atmospheric Science and Meteorological Research Center, Tehran, Iran
[3] Associate Professor, Department of earth science, Science and Research Branch, Islamic Azad University, Tehran, Iran.

(Received: 28 August 2018, Accepted: 25 June 2019)

Abstract

We studied the Iran precipitation anomaly in September to November of 2016 and its probable connection with ENSO (El Nino-Southern Oscillation). This period with similar cases in the previous 55 years (1964, 1983, and 1995 according to forecasting center of NOAA) was investigated. In all cases, ENSO changed from strong El-Nino to weak La-Nina after a very brief neutral period. In the following, observational data from 44 synoptic stations of Iran, which have long term statistics about 30 years duration, have been used. Moreover, NCEP-NCAR reanalysis data, which include mean sea level pressure, geopotential height at 850, 500 and 300 hPa, wind and humidity at 850 hPa as well as 300 hPa zonal and meridional winds have been used. Results show that along the establishment of weak La Nina after strong El Nino, autumn rainfall decreases strongly so that severe negative precipitation anomaly (up to 100%) happens in more than 70% of synoptic stations. Besides, atmospheric anomaly patterns in these conditions suggest the development and establishment of a high-pressure system over Iran so that when Siberian high pressure system strengthens, it blocks the passage of precipitation systems reaching Iran and causes cold and dry air mass establishment in the country. Moreover, during these period, extensions of subtropical high over Saudi Arabian, North African high and eastward expansion of Azores high as well as weakening of Iceland low pressure, stop the activity of Mediterranean low-pressure and Sudanese systems. At this time, the transport of moisture has also decreased relative to long term mean.

Keywords: Weak La Nina, Strong El Nino, Precipitation anomaly, Atmospheric circulation, Iran

*Corresponding author: aranjbar@gmail.com

1 Introduction

Iran is located in subtropical area and in dry belt of the globe. Therefore, its weather is influenced by subtropical mid-latitude systems. Low amount of precipitation in a large area of the country and variability of yearly precipitation in these areas, has led to destructive consequences in different areas such as agriculture, environment and water resources. For this reason, studying the variability of precipitation and its effective factors are interesting for researchers. One concerning issue to estimate the variability of climate in recent years is the analysis of precipitation variability and atmospheric circulations in different parts of the world related to teleconnection patterns. Teleconnection phenomena have their own extremes as well as stable energy sources. The most stable energy sources of the world belong to the oceans, and the most important teleconnection phenomena occur in the oceans. Clearly, these phenomena do not have a constant period of time and their severity varies in each period. One of these teleconnection phenomena is El Nino-Southern oscillation (ENSO), which is the dominant phenomena of climate variability in the multi-year scale. ENSO teleconnection exhibits temperature variability in tropical areas of the Pacific Ocean and happens nearly every five years (two to seven years). Warm phases (El Nino) have high air pressure in western tropical Pacific Ocean and cold phase (La Nina) low air pressure in the west of the ocean. El Nino and La Nina are normal climatic patterns that are formed by interaction between ocean and atmosphere. Both of them are associated with the sea surface temperature anomaly and lead to different atmospheric conditions in the world. Finding the reasons of the inevitable effects of these phenomena on the atmospheric and climatic patterns in the globe has always been in the center of researchers' attention. As an example, Hendon (2003) by using the observational data in the period of 1957-97 analyzed the relationship between ENSO and Indonesia precipitation as well as sea surface temperature and abnormalities of atmospheric circulation and showed that abnormalities of the dry season are spatially coherent and also extremely coherent to sea surface temperature and the warm phase of ENSO (El Nino). Drought conditions usually happen in the El Nino period and in this phase, sea surface temperature around Indonesia becomes colder and WALKER circulation becomes weaker. The reverse of this behavior happens in the cold phase of ENSO, which is non-coherent spatially, and there is no correlation with water surface temperature. Bhanu Kumar et al. (2004) studied the influence of Southern Oscillation and SSTs over Nino-3.4 region on the winter monsoon rainfall over coastal Andhra Pradesh. They used the mean monthly data for 124 years, and concluded that, the relationship between the Southern Oscillation index in September and the winter monsoon rainfall (WMR) over Coastal Andhra Pradesh (CAP) is variable and non-stationary. Lim and Kim (2007) analyzed the effects of ENSO on changes of the spatial and temporal variation of precipitation and Asian summer monsoon related to synoptic quantities and concluded that monsoon responds to different phases of ENSO in a complex manner. Ahmadi Givi and Parhizkar (2008) analyzed the effects of ENSO on annual precipitation between 1971 and 2000 in Iran. Their results showed that in none of the phases, annual precipitation obeys any specific rule or pattern. Feldi and Roe (2010) investigated the synoptic patterns associated with intense ENSO rainfall in the southwest of United States, and find that heavy rainfall events in the southwest arise from the presence of a persistent offshore trough and

simultaneous establishment of a strong source of subtropical water vapor; also greater intensity of these storms during La Nina is consistent with a deeper offshore trough leading to strengthened moisture fluxes. Poulomi Gangulim and Janga Reddy (2013) investigated the role of ENSO-based climate variability in modulating multivariate drought risks in the drought-prone region of Western Rajasthan in India. Their results suggested that the inclusion of ENSO-based climate variability is helpful in knowing the associated drought risks and useful for management of water resources in the region. Whelan et al. (2013) carried out the synoptic and dynamical analyses of ENSO extreme events over Australia and they concluded that synoptically, the circulation over Australia often changes significantly during La Nina events. In strong La Nina periods, there are often persistent low-pressure systems over Australia during flooding periods, replacing or displacing the typical high-pressure system seen in neutral or El Nino conditions. Barriopedro et al. (2014) studied the relationships of ENSO, sudden stratospheric warming (SSW) and tropospheric blocking. Results showed that Europe and Atlantic blocking events tend to occur before the SSW in La Nina phase, while the blocks events of the East Pacific area and Siberia occur before the SSW in La Nina phase. Shaman (2014) analyzed seasonal impacts of ENSO on Europe precipitations and concluded that ENSO has low impact on winter precipitation. Zheleznova and Gushchina (2015) studied the response of global atmosphere circulation of two types of El Nino and showed that the signal coming into the atmosphere from the heat source in the ocean propagates from the tropics to the midlatitudes symmetrically relative to the equator in the years of the canonical event of ENSO and asymmetrically in the years of the ENSO Modok. Shimizu and Ambrizzi (2015) studied the effect of ENSO on precipitation and temperature in the US and proved that precipitation and temperature are influenced by ENSO. Yao et al. (2016) analyzed extreme intraseasonal rainfall events during January–March 2010 over eastern China. They investigated two active intraseasonal rainfall periods and the physical mechanisms responsible for the onset of the two rainfall events. In the first event, anomalous ascending motion was triggered by vertically integrated (1000–300 hPa) warm temperature advection. In the second event, anomalous convection was triggered by a convectively unstable stratification, which was caused primarily by anomalous moisture advection in the lower troposphere (1000–850 hPa) from the Bay of Bengal and the Indo-China Peninsula. Alizadeh (2017) studied contrasting global teleconnection features of the eastern Pacific and central Pacific El Nino events. He concluded that, with some exceptions, the Easter Pacific (EP) El Nino and La Nina have generally similar teleconnection patterns with the reversed sign, while in some parts of the globe, different and occasionally contrasting teleconnections of the EP and Central Pacific (CP) El Nino events are identified. Singh et al. (2017) have investigated the relationship between extreme northeast (NE) monsoon rainfall (NEMR) over the Indian peninsula region and El Nino forcing. They suggested two different cases of El Nino's for analysis, based on the standardized NEMR index and Nino 3.4 index with case-1 being both Nino-3.4 and NEMR indices greater than +1 and case-2 being Nino-3.4 index greater than +1 and NEMR index less than −1. Composite analysis shows that SST anomalies in the CP and EP are strong in both cases, but large differences are noted in the spatial distribution of SST over the Indo-western Pacific region. Zheleznova and Gushchina (2017) investigated the Hadley and Walker circulation anomalies associated with the two types of El Nino.

Their research showed that the EP El Nino is characterized by the suppressed convection over the Maritime Continent and by the intensification of ascending motions in the central and eastern Pacific. The CP El Nino is characterized by the double Walker circulation cell with ascending motions in the central Pacific and descending motion on the western and eastern Pacific.

Table 1: Historical ENSO episodes (http://cpc.ncep.noaa.gov).

Year	DJF	JFM	FMA	MAM	AMJ	MJJ	JJA	JAS	ASO	SON	OND	NDJ
1963	-0.4	-0.2	0.2	0.3	0.3	**0.5**	**0.9**	**1.1**	**1.2**	**1.3**	**1.4**	**1.3**
1964	**1.1**	**0.6**	0.1	-0.3	**-0.6**	**-0.6**	**-0.6**	**-0.7**	**-0.8**	**-0.8**	**-0.8**	**-0.8**
1965	**-0.6**	-0.3	-0.1	0.2	**0.5**	**0.8**	**1.2**	**1.5**	**1.9**	**2**	**2**	**1.7**
1966	**1.4**	**1.2**	**1**	**0.7**	0.4	0.2	0.2	0.1	-0.1	-0.1	-0.2	-0.3
1967	-0.4	-0.5	-0.5	-0.4	-0.2	0	0	-0.2	-0.3	-0.4	-0.3	-0.4
1968	-0.6	-0.7	-0.6	-0.4	0	0.3	0.6	0.5	0.4	**0.5**	**0.7**	**1**
1969	**1.1**	**1.1**	**0.9**	**0.8**	**0.6**	0.4	0.4	**0.5**	**0.8**	**0.9**	**0.8**	**0.6**
1982	0	0.1	0.2	**0.5**	**0.7**	**0.7**	**0.8**	**1.1**	**1.6**	**2**	**2.2**	**2.2**
1983	**2.2**	**1.9**	**1.5**	**1.3**	**1.1**	**0.7**	0.3	-0.1	**-0.5**	**-0.8**	**-1**	**-0.9**
1984	**-0.6**	-0.4	-0.3	-0.4	-0.5	-0.4	-0.3	-0.2	-0.2	**-0.6**	**-0.9**	**-1.1**
1985	**-1**	**-0.8**	**-0.8**	**-0.8**	**-0.8**	**-0.6**	**-0.5**	**-0.5**	-0.4	-0.3	-0.3	-0.4
1986	-0.5	-0.5	-0.3	-0.2	-0.1	0	0.2	0.4	**0.7**	**0.9**	**1.1**	**1.2**
1987	**1.2**	**1.2**	**1.1**	**0.9**	**1**	**1.2**	**1.5**	**1.7**	**1.6**	**1.5**	**1.3**	**1.1**
1988	**0.8**	**0.5**	0.1	-0.3	**-0.9**	**-1.3**	**-1.3**	**-1.1**	**-1.2**	**-1.5**	**-1.8**	**-1.8**
1989	**-1.7**	**-1.4**	**-1.1**	**-0.8**	**-0.6**	-0.4	-0.3	-0.3	-0.2	-0.2	-0.2	-0.1
1990	0.1	0.2	0.3	0.3	0.3	0.3	0.3	0.4	0.4	0.3	0.4	0.4
1991	0.4	0.3	0.2	0.3	**0.5**	**0.6**	**0.7**	**0.6**	**0.6**	**0.8**	**1.2**	**1.5**
1992	**1.7**	**1.6**	**1.5**	**1.3**	**1.1**	**0.7**	0.4	0.1	-0.1	-0.2	-0.3	-0.1
1993	0.1	0.3	0.5	0.7	0.7	0.6	0.3	0.3	0.2	0.1	0	0.1
1994	0.1	0.1	0.2	0.3	0.4	0.4	0.4	0.4	**0.6**	**0.7**	**1**	**1.1**
1995	**1**	**0.7**	**0.5**	0.3	0.1	0	-0.2	**-0.5**	**-0.8**	**-1**	**-1**	**-1**
1996	**-0.9**	**-0.8**	**-0.6**	-0.4	-0.3	-0.3	-0.3	-0.3	-0.4	-0.4	-0.4	-0.5
2010	**1.5**	**1.3**	**0.9**	0.4	-0.1	**-0.6**	**-1**	**-1.4**	**-1.6**	**-1.7**	**-1.7**	**-1.6**
2011	**-1.4**	**-1.1**	**-0.8**	**-0.6**	**-0.5**	-0.4	**-0.5**	**-0.7**	**-0.9**	**-1.1**	**-1.1**	**-1**
2012	**-0.8**	**-0.6**	**-0.5**	-0.4	-0.2	0.1	0.3	0.3	0.3	0.2	0	-0.2
2013	-0.4	-0.3	-0.2	-0.2	-0.3	-0.3	-0.4	-0.4	-0.3	-0.2	-0.2	-0.3
2014	-0.4	-0.4	-0.2	0.1	0.3	0.2	0.1	0	0.2	0.4	**0.6**	**0.7**
2015	**0.6**	**0.6**	**0.6**	**0.8**	**1**	**1.2**	**1.5**	**1.8**	**2.1**	**2.4**	**2.5**	**2.6**
2016	**2.5**	**2.2**	**1.7**	**1**	**0.5**	0	-0.3	**-0.6**	**-0.7**	**-0.7**	**-0.7**	**-0.6**

Angel and Valcarcel (2018) studied teleconnections between ENSO and rainfall and drought in Puerto Rico. Their results indicate that ENSO is not a main

factor causing droughts in Puerto Rico for the period of study and thus should not be a factor in predicting the potential for local dry periods or large precipitation deficits in the future. Thus, local drought prediction efforts should be focused on finding major causes of local rainfall variation other than ENSO.

According to forecasting center of NOAA, ENSO phenomena exerts influence on precipitation frequencies. Thus, it is important to study Iran precipitation anomalies according to ENSO phenomena. Therefore, in this research, the focus is on the analysis of probable relationships of dry autumn and ENSO. In this study, the reasons for the fall drought in events that ENSO changes from strong El-Nino signal to weak La-Nina phase after a very brief neutral period is investigated. In the period of 1960 to 2017, four such cases are found according to the data of the forecasting center of NOAA. For this selection see also Table 1.

2 Database

2 -1 ENSO factor

There are some factors to describe ENSO phenomena and its conditions, such as Southern Oscillation index (SOI, Trenbert, 1984), and multivariate ENSO indices (MEI, Wolter and Timlin; TNI, Trenbert and Stepaniak, 2001). In this research, oceanic Nino index (ONI) that is developed by climate prediction center (CPC) from NOAA, is used to describe the different conditions of ENSO. It should be mentioned that using other indices such as SOI and MEI would not make any specific difference in the results (Penalba and Rivera, 2016).

2-1 Methodology

For the analysis, at first, La Nina years are taken from the CPC for the period of 1960 - 2017 (Table 2). In this period, the years that have exactly had the conditions described in the previous section for the fall season (changing from strong El-Nino episode after a very brief neutral period to weak La-Nina) were selected. These years are 1964, 1983, 1995 and 2016.

Monthly average rainfalls were collected from the Department of Meteorology for 44 synoptic stations to identify the precipitation anomaly (Figure 1). Besides, a 30-year period (1981-2010) taken as the climatic period is considered. Further, reanalysis data of NOAA center in different levels were used for synoptic study. Data includes mean sea level pressure, geopotential height at 850, 500 and 300 hPa, 850 hPa moisture flux, and 300 hPa zonal and meridional wind. These data were used to estimate monthly mean and perturbation components of pressure, geopotential height, wind and humidity parameters, and jet streams, compared to the long-term period. The years were selected according to the domination of ENSO phenomena for fall season with the conditions mentioned (1964-1983-1995, 2016). As already stated, the data for these cases were extracted from the climate prediction center (CPC) and are available at http://www.cpc.ncep.noaa.gov. In the following, GIS software was used to draw precipitation maps. For calculation of precipitation anomaly related to the

Table 2: La Nina periods (Sep-Oct-Nov) during the 1960-2017.

1964	1970	1971	1973	1974	1975	1983	1984	1988
1995	1998	1999	2000	2007	2010	2011	2016	2017

Figure 1: Location of selected weather stations.

long-term mean, Equation (1) is used:

$$\overline{P} = \frac{1}{30}\sum_{i=1}^{30} p_i. \quad (1)$$

where P_i and P are i^{th} year seasonal precipitation and mean seasonal precipitation for the desired station respectively. The seasonal precipitation anomaly is calculated according to:

$$\left(\frac{p-\overline{p}}{\overline{p}}\right) * 100. \quad (2)$$

For the calculation of pressure anomaly patterns, the amount of perturbation for each pattern was calculated. A general meteorological quantity A is divided into the average $\overline{A}$ and perturbation $\acute{A}$ parts:

$$A = \bar{A} + A\acute{}. \quad (3)$$

For this purpose, 30-year averages of mean sea level pressure, 850, 500 and 300 hPa geopotential height, 850 hPa wind, specific humidity and 300 hPa wind are taken as average values, and differences of the latter quantities with respect to the long-term average are taken as the perturbation.

3 Results

3-1 Precipitation abnormality

According to Equations (1) and (2), mean seasonal precipitation for the long term and selected years as well as precipitation anomaly in all synoptic stations were calculated. Calculations showed negative anomaly for 76% of Iran synoptic stations in 2016 fall. Calculations were done for years with similar conditions according to the ENSO factor (1964, 1983 and 1995). Results showed severe precipitation anomaly in different locations. Figure 2 shows the precipitation anomaly of Iran and distribution of fall precipitation abnormality in 1964 relative to the long-term mean. This figure shows that, with the exception of two small parts in the northeast experienced increases by 23.69 and 17.45%, in the other parts, severe negative anomaly was dominant and a dry fall was experienced. Moreover, fall precipitation anomaly in 1983 showed that all stations had lower precipitation relative to the long-term mean. The amount of precipitation anomaly in all parts of the country was

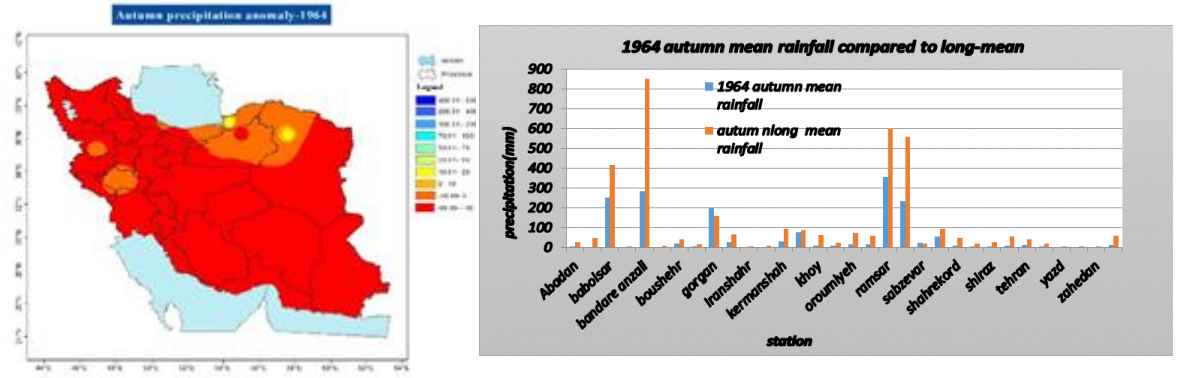

Figure 2: Distribution of autumn precipitation (value and anomaly) of the weather stations in 1964 relative to the long-term mean.

more than 50 percent. Therefore, in 1983 a very dry fall dominated in Iran (Figure 3). In 1995, with the exception of a small area in the south, in the rest of the regions precipitation had decreased from 4% in the north up to 100% in the south (Figure 4). In 2016, only 14% of the whole area located in the south had normal or above normal precipitation, while the rest of the country experienced a very dry fall relative to the long-term mean (Figure 5).

3-2- Pressure patterns anomaly

First case: 2016 fall (September till November)

Figure 6 shows the anomaly pattern of monthly mean sea level pressure in hPa, 500 and 850 hPa levels, geopotential height in gpm and moisture flux of 850 hPa in 2016 for September to November. Analysis of sea level pressure map shows that Siberian high pressure ridge is stretched from the northeast to the southwest of Iran, and by the northeast-southwest axis covers almost all of the country. This high pressure center has a significant increase in Caspian shores (about 4 hPa), and its ridge covers much of the country. At this time, the analysis of sea level pressure anomaly shows that an increase in the north half of Iran by about 2 hPa relative to the long-term mean, and there is no change in the south half. The 850 hPa Icelandic low-pressure center has increased by about 80 gpm in Europe. The Arabian high-pressure remains with no change but its north-south elongation stops the activity of Sudanese low pressure, and prevents entering its reaching to the south and southwest of Iran. North African high is strengthened and displaced to the north and affects center and east of the Mediterranean Sea, which prevents the formation of Mediterranean trough. Thus, the dominance of Siberian high pressure

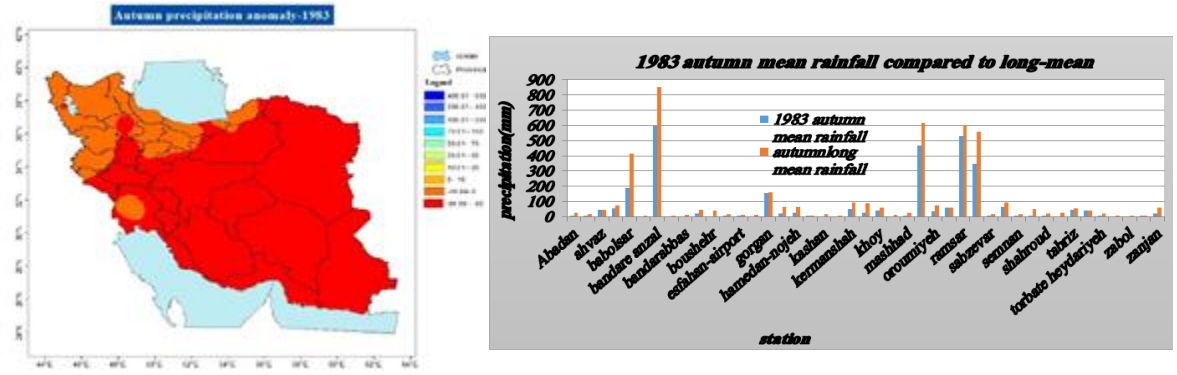

Figure 3: The same as Figure 2 but for 1983.

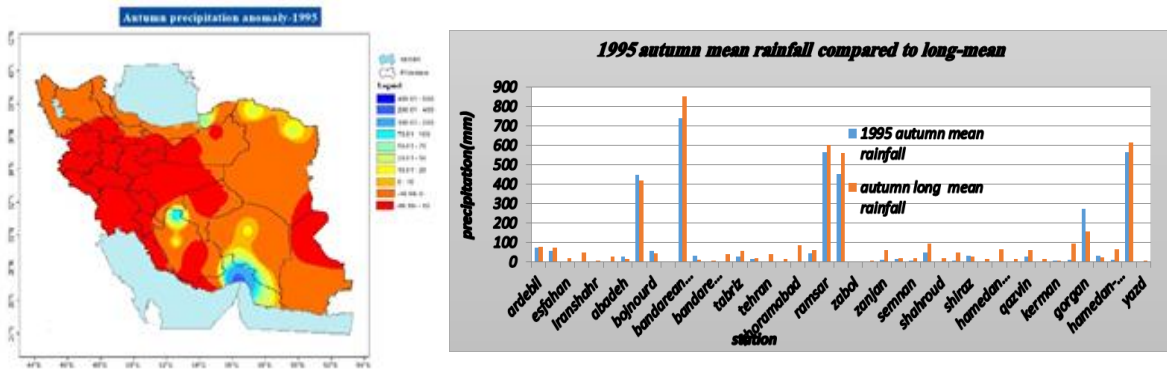

Figure 4: The same as Figure 2 but for 1995.

over Iran, weakening of Mediterranean storm track, strength and existence of African high, weakening of the Iceland low-pressure center and northward expansion of the Arabian high in the south, which prevent the entrance of Sudan's trough to the southwest of Iran, all make condition to form an extreme negative precipitation anomaly in these periods.

In the mid-latitude, the 5880 gpm contour at 500 hPa level is formed in Saudi Arabia and south of the Persian Gulf around the 20 to 30 latitudes. The 5840 gpm contour line has extended northward to 33 degrees latitude and a ridge is located in these areas.

Iceland low increase by about 60 gpm at 500 hPa level and has weakened substantially. In the eastern part of Mediterranean Sea, geopotential height has increased by about 40 gpm relative to the long-term mean and the currents are zonal. Positive anomaly of geopotential height over east of the Mediterranean means weakness of the Mediterranean trough and consequently the associated storm track. Therefore, in the absence of Mediterranean trough, zonal currents and strong positive height abnormality in the mid-latitudes and the existence of subtropical high ridge over Iran plateau have contributed to Iran's negative precipitation anomaly. At 850 hPa level, the moisture flux map shows that the humidity at Red Sea has decreased by about 0.2 g/kg and at Mediterranean Sea by about 0.8 g/kg. The current vectors over the Red Sea and the Mediterranean Sea are eastward and abnormal. The moisture flux map shows clearly that Iran is influenced by the northern cold and dry current from Siberia. Therefore, the absence of sufficient moisture and the southward extension of the northerly cold and dry currents caused severe low precipitation in 2016 fall in Iran.

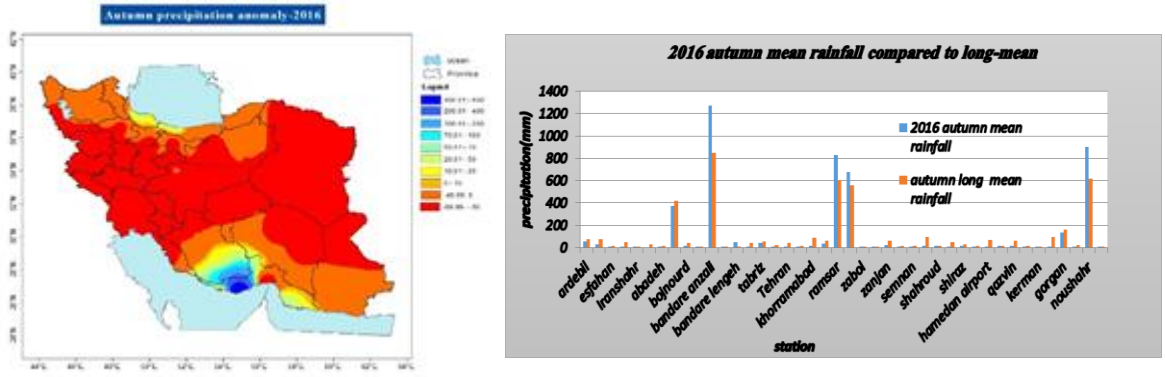

Figure 5: The same as Figure 2 but for 2016 fall.

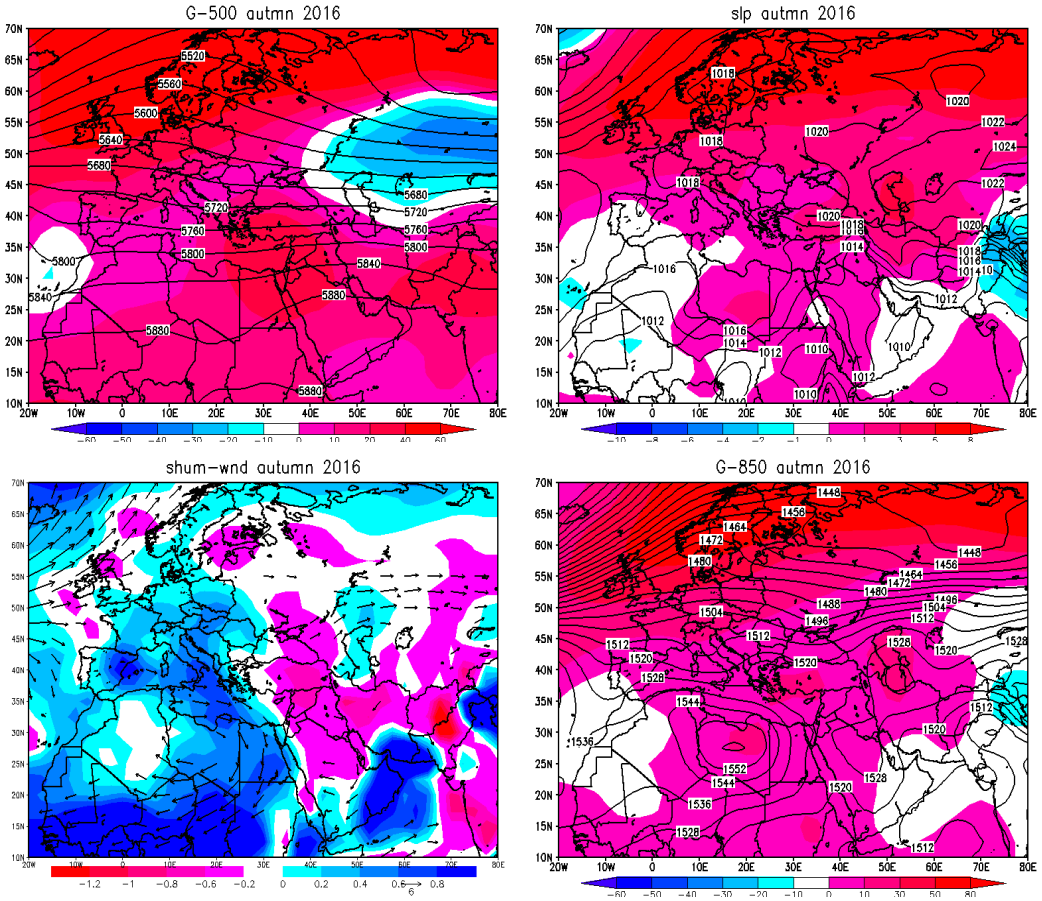

Figure 6: Monthly average sea level pressure in hPa and anomaly (colored amounts) and amount of 850 and 500 hPa average geopotential height in geopotential meter (gpm) and anomaly (colored amounts) and 850 hPa level moisture flux anomaly in g/kg (September to November 2016).

Second case: 1995 fall (September till November)

In sea level pressure map, it is clear that Siberian high have developed and spread toward Iran in such a way that has almost covered the country. The Arabian high-pressure center is located in the southwest of the Persian Gulf, which is developed toward the north, and its ridges prevent the development of Sudanese low pressure. The Mediterranean Sea is influenced by Azores high pressure, which is developed toward the north and east and its ridges cover almost all of the Mediterranean Sea. In the north of Europe, Iceland low-pressure center is strengthened. Therefore, the existence of Siberian high along with the Arabian high center at 850 hPa level, which is developed up to 33 degrees north and stops eastern reinforcement of Sudanese low, and also eastern development of the Azores high that stops the formation of Mediterranean trough and weakening of the Iceland low center in the north of Europe (Figure7) are all influential patterns of the 1995 drought. Moreover, the moisture flux map shows that the amount of incoming moisture flux to Iran has a reduction of 1.2 g/kg relative to the long-term mean.

Third case: 1983 fall (September till November)

Siberian high pressure has entered Iran from the east and covered all of the southwest of the country so that its ridges have linked with the Arabian high pressure. The central pressure in Sudanese low and in the west of the Mediterranean Sea has decreased by about 2 hPa relative to the long-term

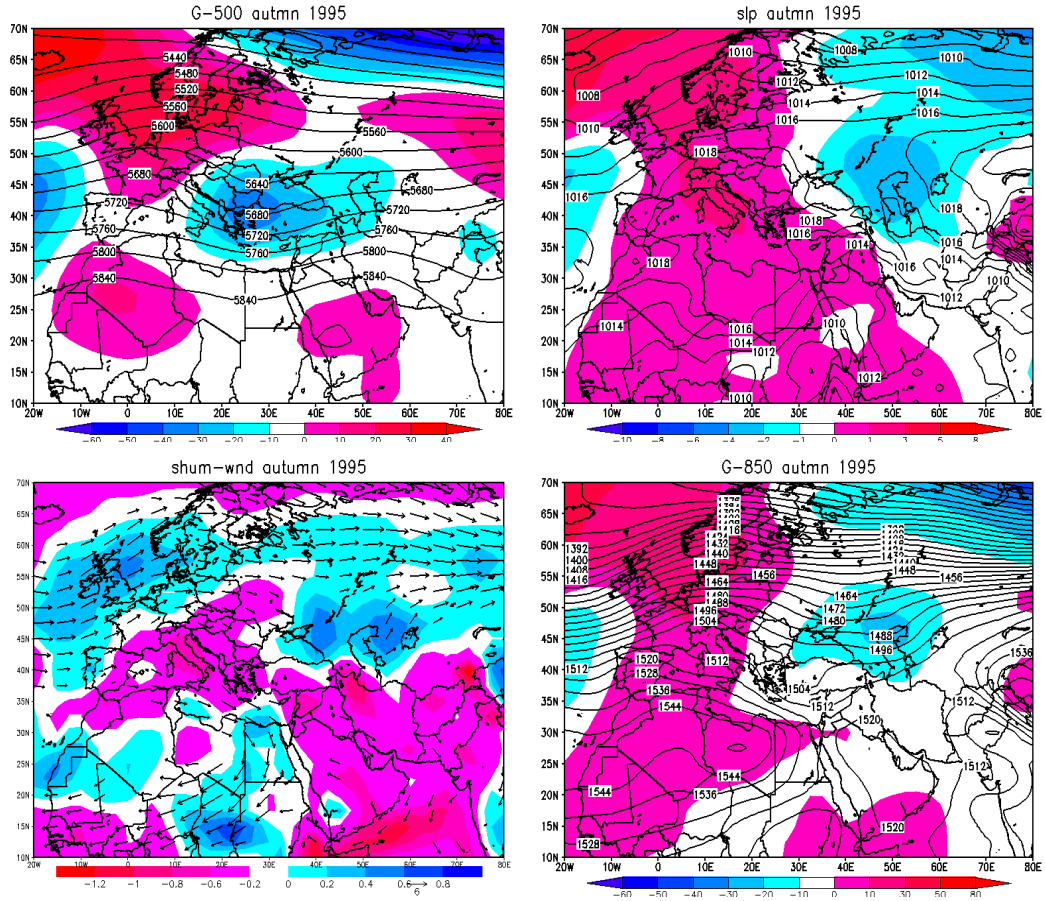

Figure 7: The same as Figure 6 but for case of September to November 1995.

mean. At 850 hPa, the center of the Azores high has reinforced and expanded to the north and east, so that its ridges have spread to the Mediterranean region. Besides, the Mediterranean Sea is influenced by Azores high pressure and Siberian high from east and west, such that the Mediterranean trough is not formed. In mid-latitudes, subtropical high is reinforced and expanded up to 37 degrees latitude, thus preventing the weather systems entering Iran. Iceland low gets weak and acts like a high. Thus, the existence of Siberian high pressure in the northeast, which covers all of Iran and east of the Mediterranean Sea, beside the eastern development of the Azores high pressure toward the west and weakening of Iceland low, which stops the formation of the Mediterranean trough, as well as the reinforcement and northern development of subtropical high are determining patterns in the 1983 fall drought (Figure 8).

Fourth case: 1964 fall (September till November)

In 1964, Iran is influenced by pressure belt of Siberia, Africa, the Azores and Iceland. Siberian high pressure is developed and stretched towards Iran plateau from east and northeast. Azores high pressure has been reinforced to the north and northeast and cover the whole of the Mediterranean Sea and merged with the North African high pressure. The northwest of Iran is influenced by a migrating low pressure, but its central pressure is severely reduced relative to the long-term mean, its troughs cover some parts of the eastern Mediterranean as seen in Figure 9, and little amounts of humidity from the east of the Mediterranean and the Red Sea are

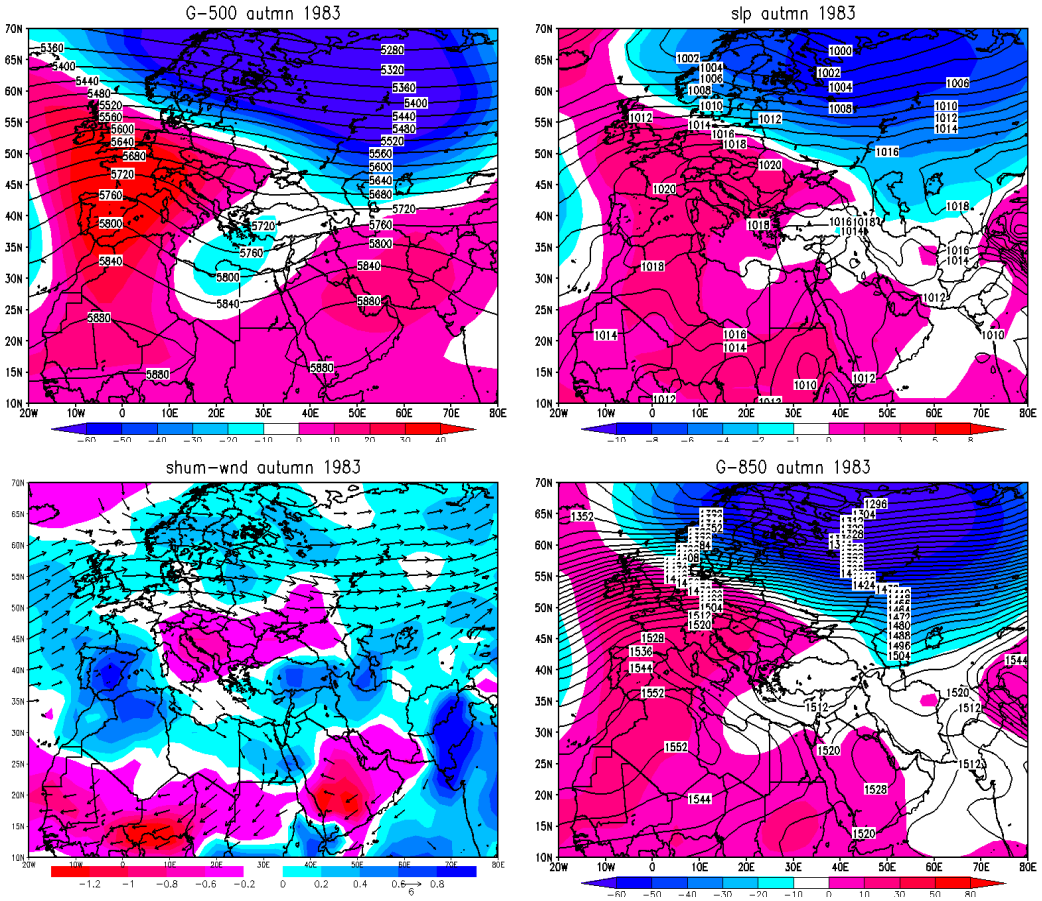

Figure 8: The same as Figure 6 but for case September to November 1983.

transported to small areas of the northwest and north of Iran. However, the rest of Iran suffers a very significant reduction in the moisture receiving from the latter seas. The most amount of decrease is related to the south of Iran, which is more than 1.2 g/kg. Therefore, as a result of the lack of Mediterranean trough formation that caused eastern development of the Azores high pressure, covering huge parts of the west and center of the Mediterranean Sea, and weakness of Iceland low in the north of Europe, great parts of Iran experienced drought in autumn of 1968.

4 300 hPa level geopotential height and jet streams

ENSO, as the dominant pattern of interannual climate variability, has strong influences on the atmospheric circulation around the globe (e.g., Bjerknes, 1969; Horel and Wallace, 1981; Trenberth et al., 1998). Much of climate variability such as that due to ENSO is often linked to recurring jet streams, ocean temperature, and rainfall patterns. In this section, the composite maps of 300 hPa jet stream and geopotential height, to determine upper-tropospheric troughs, have been drawn and inactivity of the effective rainfall systems has been investigated. As Figure 10 shows, in 1964 the subtropical jet stream axis with an anticyclonic curvature located at latitudes higher than the long-term mean (30 to 35 degrees latitude). Mediterranean trough is weak and prevents weather disturbances entering Iran. Further, the existence of ridges on the northern Europe states that the Iceland low cannot be strengthened. In 1983 and 1995, subtropical jet stream with anticyclonic axis located on Iran.

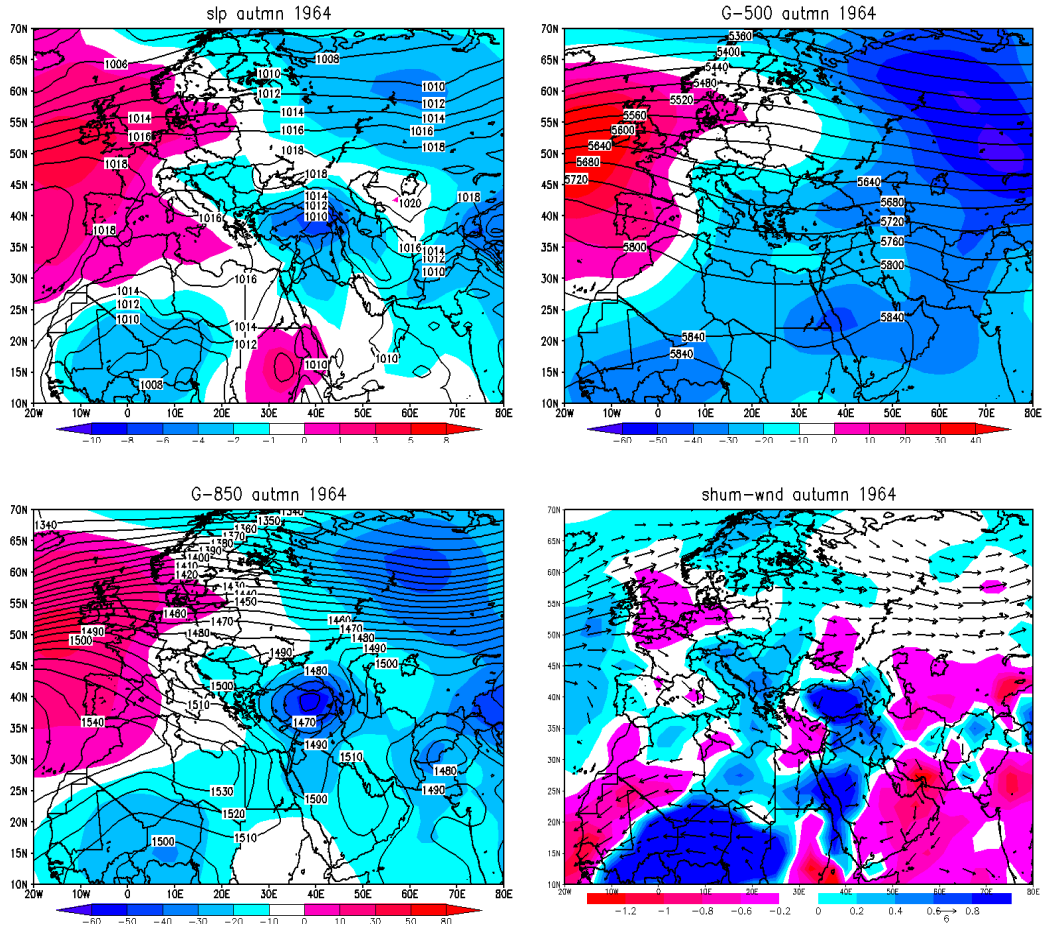

Figure 9: The same as Figure 6 but for case September to November 1964.

Also as Figure 11 shows, although Mediterranean trough is formed, its location on the northwest flank of the jet entrance leads to cold and dry air (see Bell, 2013). On the other hand, the existence of northern Europe high and establishment of subtropical jet ridges over the country prevent weather systems entering Iran (as the moisture flux map clearly shows in Figure 8). The ridges on northern Europe are present in 2016 too, and are stronger than other cases; the subtropical jet stream is slightly stronger and shifted further to the east, so that, Mediterranean region and Iran are located at the entrance of the jet stream axis, which lead to the intrusion of cold and dry air.

5 Conclusions

Results of the analysis shows that when La Nina is weak in autumn and occurs after a strong El Nino, it is changed in a very brief neutral phase of ENSO, drought occurs in the fall season in Iran. In order to analyze this, four cases were identified obeying these conditions, and rainfall anomalies were calculated in these cases. Results show that in this condition, precipitation reduces in the center, east, southeast, west and also northwest of Iran, and a very dry fall dominates in these parts. In all analyzed years, most of Iran experiences a negative precipitation abnormality of more than 60%. Besides, synoptic studies for the selected cases were conducted. It showed that fall droughts caused by weak and short La Nina dominance after a severe El Nino are controlled by six major pressure patterns. These major patterns are: Arabian and North African

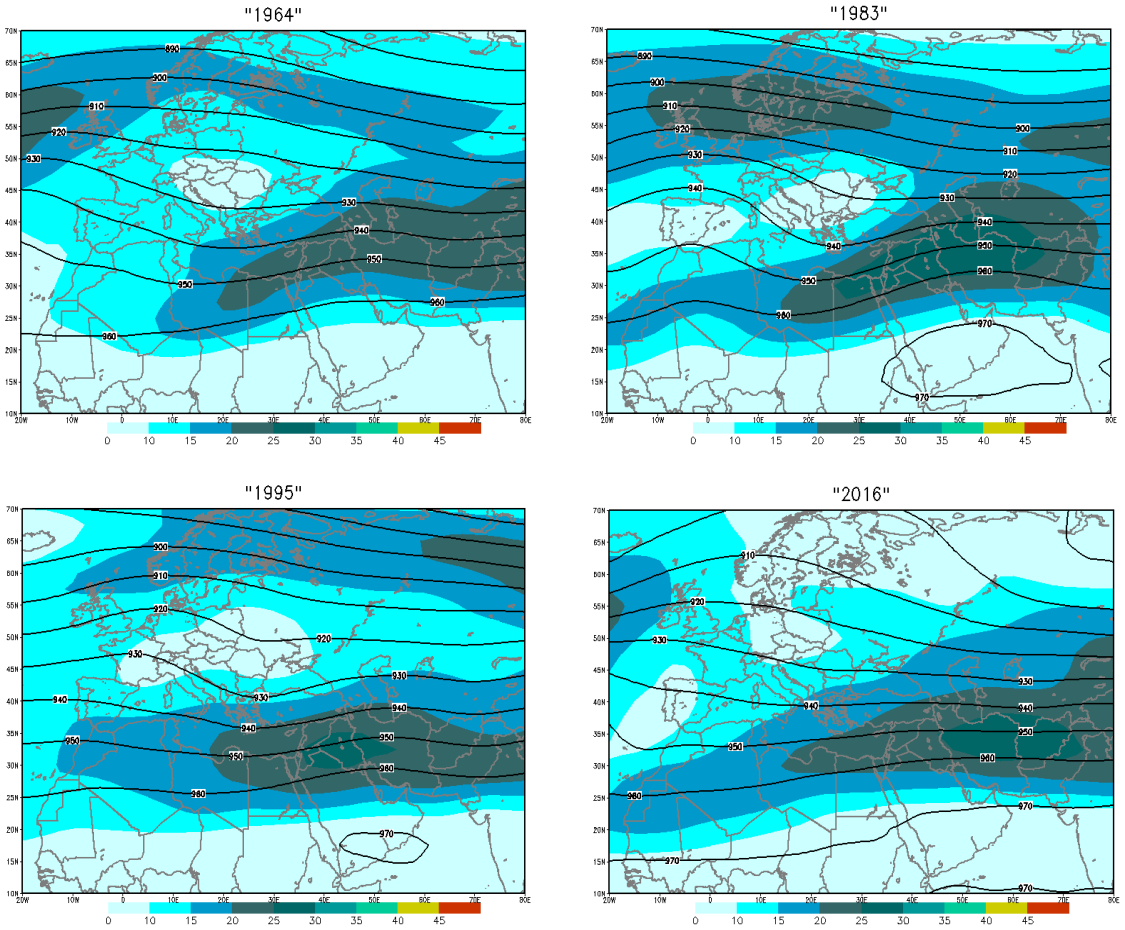

Figure 10: 300 hPa geopotential height and jet stream (Sep. to Nov. 1964-1983-1995, 2016).

subtropical high pressure, Siberian high pressure, Azores high pressure, Mediterranean low pressure and Iceland low. When ridges of Arabian high pressure develop towards the north, they prevent eastward movement of Sudanese low pressure. The ridges of this pressure center may develop to higher latitudes and prevent the Mediterranean weather disturbance entering Iran from the west, so the Mediterranean storm track is displaced to higher latitudes. The development of African high pressure towards the south and east of the Mediterranean Sea and development of the Azores high pressure ridges towards

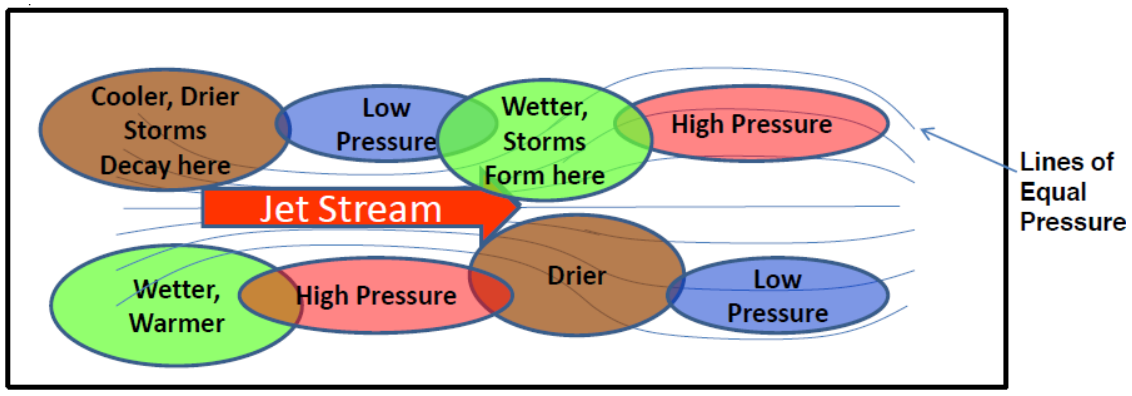

Figure 11: Jet stream-related patterns of air pressure, storminess, precipitation and temperature (Bell, 2013).

north and east, and covering its ridges on the center and west of the Mediterranean Sea, causes the weakness or lack of formation of the Mediterranean trough. The most common pattern among the patterns determining drought in the years studied is the increase of central pressure of Iceland low-pressure center in the north of Europe, which its reinforcement or weakness, effects Mediterranean low pressure. Therefore, the existence of Siberian high pressure in the north, which causes the development of dry and cold air in Iran, the existence of Arabian, North African and Azores high pressures, and certainly the weakening of the Iceland low center respectively block incoming disturbances of Sudanese low pressure and prevent the formation of Mediterranean trough. At 300 hPa, composite maps of geopotential height and jet stream show, for the four cases, the establishment of subtropical jet stream axis of anticyclonic curvature over Iran and positioning of the Mediterranean region on the northwest of jet entrance are the factors that prevent the effective system acting on Iran's rainfall. Further, the 850 hPa moisture flux maps confirms the lack of sufficient moisture transport to Iran in the fall season in the analyzed years. As a result, in the occurrence of a weak La Nina after a severe El Nino, dry autumns should be expected in Iran, especially in the center, east, southeast, west and also northwest regions. This result can be considered for seasonal forecasting in Iran.

References

Ahmadi Givi, F. and Parhizkar, D., 2008, investigation of ENSO role in Iran annual rainfall (1971-2000); **Iranian Journal of Geophysics, 2**(2), 25-37.

Alizadeh, O., 2017, Contrasting global teleconnection features of the eastern Pacific and central Pacific El Niño events, **Dynam. Atmos. Ocean, 80,** 139-154

Angel, R., Torres-Valcárcel, 2018, Teleconnections between ENSO and rainfall and drought in Puerto Rico, **Int. J. Climatol, 38**, e1190-e1204.

Barriopedro, D., Calvo, N., 2014, On the relationship between ENSO, Stratospheric Sudden Warmings and Blocking; **J. Climate, 27**, 4704-4720.

Bell, G., 2013, Flavors of Climate variability: El Nino, La Niña, Recurring Jet Stream patterns, Multi-Decadal Variability, (www.cpc.ncep.noaa.gov).

Bhanu Kumar, C.V., Naidu, S.R.L., Rao, 2004, Influence of southern oscillation and SSTs over Nino-3.4 region on the winter monsoon rainfall over coastal Andhra Pradesh, **J. Earth Syst. Sci., 113(3)**, 313–319.

Bjerknes, J., 1969, Atmospheric teleconnections from the equatorial Pacific. **Mon. Wea. Rev**., 97, 163–172.

Danielson, R.E., Gyakum, J.R. and Straub, D.N., 2006, A case study of downstream baroclinic development over the North Pacific Ocean. Part II: diagnoses of eddy energy and wave activity**. American Meteorological Society, 134**(5), 1549-1576.

Delitala, A., Cesari, D., Chesa, P., and Ward, M., 2000, Precipitation over Sardinia (Italy) during the 1946-1993 rainy season and associated large scale climate variation. **Int. J. Climatol., 20**, 519-541.

Feldi, N. and Roe, G.H., 2010, Synoptic weather patterns associated with intense ENSO rainfall in the southwest United States. **Geophys. Res. Lett., 37**(23).

Glantz, M.H., 1996, Currents of Change: El Niño's Impact on Climate and Society, Cambridge: **Cambridge University Press, Cambridge, UK**, xiii + 194 pp.

Hendon, H.H., 2003, Indonesian rainfall variability: Impacts of ENSO and local air-sea interaction. **J. Climate, 16**, 1775-1790.

Horel, J.D. and Wallace, J.M., 1981, Planetary-scale atmospheric phenomena associated with the Southern Oscillation. **Mon. Wea. Rev**., 103, 813–829, http://www.cpc.ncep.noaa.gov.

Trenberth, K.E. and Stepaniak, D.P., 2000, Indices of El Nino Evolution, **J. Climate, 14**.

Lim, Y.K., and Kim, K.Y., 2007, ENSO impact on the space–time evolution of the regional Asian summer monsoons. **J. Climate, 20**, 2397–2415.

Poulomi Gangulim and Janga Reddy, 2013, Analysis of ENSO-based climate variability in modulating drought risks over western Rajasthan in India, **J. Earth Syst. Sci., 2013, 122**(1), 253–269.

Shaman, J., 2014, The seasonal effects of ENSO on European precipitation: Observational analysis. **J. Climate. 27(3),** 1010-1028.

Singh, P., Gnanaseelan, C. and Chowdary, J.S., 2017, North-East monsoon rainfall extremes over the southern peninsular India and their association with El Niño, **Dynam. Atmos. Ocean, 80**, 1-11.

Shimizu, M. and Ambrizzi, T., 2015, MJO influence on ENSO effects in precipitation and temperature over South America, **Theor. Appl. Climatol., 124(1–2)**, 291–301.

Trenberth, K.E., Branstator, G.W. Karoly, D., Kumar, A., Lau, N.-C. and Ropelewski, C., 1998, Progress during TOGA in understanding and modeling global tele-connections associated with tropical sea surface temperatures. **J. Geophys.** Res., 103, 14 291–14 324.

Troccoli, A., 2010, Seasonal climate forecasting, **Meterol. Appl., 17**, 251–268.

Penalba, O.C., & Rivera, J.A., 2016, Precipitation response to El Niño/La Niña events in Southern South America – emphasis in regional drought occurrences, **Adv. Geosci., 42**, 1–14.

Viles, H.A., and Goudie, A.S, 2003, International, decadal and multidecadal scale climatic variability and geomorphology**. Earth Sci Rev., 61**, 105-131.

Whelan, J.A., Frederiksen, J.S., Frederiksen, C.S. and Osbrough, S.L, 2013, Synoptic and dynamical analyses of ENSO extreme events over Australia, 20th International Congress on Modelling and Simulation, **Adelaide, Australia, 1–6 December 2013**.

Yao, S. and Huang, Q., 2016, An analysis of extreme intraseasonal rainfall events during January–March 2010 over eastern China**, Dynam. Atmos. Ocean, 75,** 22-32.

Zheleznova, I.V., and Gushchina, D.Yn, 2015, The response of global atmospheric circulation to two types of El Niño. **Russ. Meteorol. Hydrol., 40**, 170-179.

Zheleznova, I.V., and Gushchina, D.Yn., 2017, Hadley and Walker circulation anomalies associated with the two types of El Niño. **Russ. Meteorol. Hydrol, 42**, 625-634.